Research Article | Vol. 26, No. 18 | 3 Sep 2018 | OPTICS EXPRESS A729
Optics EXPRESS

Dynamic optical control of near-field radiative transfer

JUNLONG KOU, AND AUSTIN J. MINNICH*

Division of Engineering and Applied Science, California Institute of Technology, Pasadena, California 91125, USA
*aminnich@caltech.edu

Abstract: Dynamic control of radiative heat transfer is of fundamental interest as well as for applications in thermal management and energy conversion. However, realizing high contrast control of heat flow without moving parts and with high temporal frequencies remains a challenge. Here, we propose a thermal modulation scheme based on optical pumping of semiconductors in near-field radiative contact. External photo-excitation of the semiconductor emitters leads to increases in the free carrier concentration that in turn alters the plasma frequency, resulting in modulation of near-field thermal radiation. The temporal frequency of the modulation can reach hundreds of kHz limited only by the recombination lifetime, greatly exceeding the bandwidth of methods based on temperature modulation. Calculations based on fluctuational electrodynamics show that the heat transfer coefficient between two silicon films can be tuned from near zero to 600 $Wm^{-2}K^{-1}$ with a gap distance of 100 nm at room temperature.

OCIS codes: (350.5610) Radiation; (120.6810) Thermal effects; (240.6680) Surface plasmons.

References and links

1. T. Inoue, M. D. Zoysa, T. Asano, and S. Noda, "Realization of dynamic thermal emission control," Nat. Mater. **13**, 928–931 (2014).
2. C. R. Otey, W. T. Lau, and S. Fan, "Thermal rectification through vacuum," Phys. Rev. Lett. **104**, 154301 (2010).
3. J. Zhu, K. Hippalgaonkar, S. Shen, K. Wang, Y. Abate, S. Lee, J. Wu, X. Yin, A. Majumdar, and X. Zhang, "Temperature-gated thermal rectifier for active heat flow control," Nano Lett. **117**(13), 4867–4872 (2014).
4. K. Chen, P. Santhanam, S. Sandhu, L. Zhu, and S. Fan, "Heat-flux control and solid-state cooling by regulating chemical potential of photons in near-field electromagnetic heat transfer," Phys. Rev. B **91**(13), 134301 (2015).
5. D. Ding, T. Kim, and A. J. Minnich, "Active thermal extraction of near-field thermal radiation," Phys. Rev. B **93**, 081402 (2016).
6. X. Liu, and W. J. Padilla, "Reconfigurable room temperature metamaterial infrared emitter," Optica **4**, 430 (2017).
7. K. Ito, K. Nishikawa, A. Miura, H. Toshiyoshi, and H. Iizuka, "Dynamic modulation of radiative heat transfer beyond the blackbody limit," Nano Lett. **17**(7), 4347–4353 (2017).
8. M. A. Kats, R. Blanchard, S. Zhang, P. Genevet, C. Ko, S. Ramanathan, and F. Capasso, "Vanadium dioxide as a natural disordered metamaterial: perfect thermal emission and large broadband negative differential thermal emittance," Phys. Rev. X **3**, 041004 (2013).
9. V. W. Brar, M. C. Sherrott, M. S. Jang, S. Kim, L. Kim, M. Choi, L. A. Sweatlock, and H. A. Atwater, "Electronic modulation of infrared radiation in graphene plasmonic resonators," Nat. Commun. **6**, 7032 (2015).
10. J. F. Ihlefeld, B. M. Foley, D. A. Scrymgeour, J. R. Michael, B. B. McKenzie, D. L. Medlin, M. Wallace, S. Trolier-McKinstry, and P. E. Hopkins, "Room-temperature voltage tunable phonon thermal conductivity via reconfigurable interfaces in ferroelectric thin films," Nano Lett. **15**, 1791–1795 (2015).
11. O. Ilic, N. H. Thomas, T. Christensen, M. C. Sherrott, M. Soljacic, A. J. Minnich, O. D. Miller, and H. A. Atwater, "Active radiative thermal switching with graphene plasmon resonators," ACS Nano **12**, 2474–2481 (2018).
12. O. Ilic, M. Jablan, J. D. Joannopoulos, I. Celanovic, H. Buljan, and M. Soljacic, "Near-field thermal radiation transfer controlled by plasmons in graphene," Phys. Rev. B **85**, 155422 (2012).
13. R. Zheng, J. Gao, J. Wang, and G. Chen, "Reversible temperature regulation of electrical and thermal conductivity using liquid-solid phase transitions," Nat. Commun. **2**, 289 (2011).
14. J. Hildenbrand, J. Korvink, J. Wollenstein, C. Peter, A. Kurzinger, F. Naumann, M. Ebert, and F. Lamprecht, "Micromachined mid-infrared emitter for fast transient temperature operation for optical gas sensing systems," IEEE Sensors J. **10**, 353–362 (2010).
15. H. S. Carslaw, and J. C. Jaeger, *Conduction of Heat in Solids* (Oxford Science Publications, 1959)
16. S. Shen, A. Narayanaswamy, and G. Chen, "Surface phonon polaritons mediated energy transfer between nanoscale gaps," Nano Lett. **9**, 2909–2913 (2009).

#326902 https://doi.org/10.1364/OE.26.00A729
Journal © 2018 Received 26 Mar 2018; revised 4 Jun 2018; accepted 5 Jun 2018; published 24 Jul 2018

Optics EXPRESS

17. E. Rousseau, A. Siria, G. Jourdan, S. Volz, F. Comin, J. Chevrier, and J.-J. Greffet, "Radiative heat transfer at the nanoscale," Nat. Photon. **3**, 514–517 (2009).
18. B. Song, D. Thompson, A. Fiorino, Y. Ganjeh, P. Reddy, and E. Meyhofer, "Radiative heat conductances between dielectric and metallic parallel plates with nanoscale gaps," Nat. Nanotechnol. **11**, 509–514 (2016).
19. Y. Yang, and L. Wang, "Spectrally enhancing near-field radiative transfer between metallic gratings by exciting magnetic polariton in nanometric vacuum gaps," Phys. Rev. Lett. **117**, 044301 (2016).
20. R. St-Gelais, L. Zhu, S. Fan, and M. Lipson, "Near-field radiative heat transfer between parallel structures in the deep subwavelength regime," Nat. Nanotechnol. **11**, 515–519 (2016).
21. A. V. Shchegrov, K. Joulain, R. Carminati, and J.-J. Greffet, "Near-field spectral effects due to electromagnetic surface excitations." Phys. Rev. Lett. **85**, 1548–1551 (2000).
22. A. Karalis, and J. D. Joannopoulos, "'Squeezing' near-field thermal emission for ultra-efficient high-power thermophotovoltaic conversion," Sci. Rep. **6**, 28472 (2016).
23. M. Laroche, R. Carminati, and J.-J. Greffet, "Near-field thermophotovoltaic energy conversion," J. Appl. Phys. **100**, 063704 (2006).
24. R. Messina, and P. Ben-Abdallah, "Graphene-based photovoltaic cells for near-field thermal energy conversion," Sci. Rep. **3**, 1383 (2013).
25. B. Zhao, K. Chen, S. Buddhiraju, G. Bhatt, M. Lipson, and S. Fan, "High-performance near-field thermophotovoltaics for waste heat recovery," Nano Energy **41**, 344–350 (2017).
26. S. Basu, and M. Francoeur, "Near-field radiative transfer based thermal rectification using doped silicon," Appl. Phys. Lett. **98**, 113106 (2011).
27. S. Basu, B. J. Lee, and Z. M. Zhang, "Near-field radiation calculated with an improved dielectric function model for doped silicon," J. Heat Transfer **132**(2), 023302 (2009).
28. A. D. Dunkelberger, C. T. Ellis, D. C. Ratchford, A. J. Giles, M. Kim, C. S. Kim, B. T. Spann, I. Vurgaftman, J. G. Tischler, J. P. Long, O. J. Glembocki, J. C. Owrutsky, and J. D. Caldwell. "Active tuning of surface phonon polariton resonances via carrier photoinjection," Nature Photon. **12**, 50–56 (2018).
29. P. Guo, R. D. Schaller, J. B. Ketterson, and R. P. H. Chang, "Ultrafast switching of tunable infrared plasmons in indium tin oxide nanorod arrays with large absolute amplitude," Nature Photon. **10**, 267–273 (2016).
30. N. Kinsey, C. DeVault, J. Kim, M. Ferrera, V. M. Shalaev, and A. Boltasseva, "Epsilon-near-zero Al-doped ZnO for ultrafast switching at telecom wavelengths," Optica **2**, 616–622 (2015).
31. N. A. Krueger, A. L. Holsteen, S. Kang, C. R. Ocier, W. Zhou, G. Mensing, J. A. Rogers, M. L. Brongersma, and P. V. Braun, "Porous silicon gradient refractive index micro-optics," Nano Lett. **16**(12), 7402–7407 (2016).
32. C. R. Ocier, N. A. Krueger, W. Zhou, and P. V. Braun, "Tunable visibly transparent optics derived from porous silicon," ACS Photon. **4**(4), 909–914 (2017).
33. S. M. Rytov, *Theory of electric fluctuations and thermal radiation* (Air Force Cambridge Research Center, 1959).
34. J. C. M. Garnett, "Colours in metal glasses and in metallic films," Philos. Trans. R. Soc. London A **203**, 385–420 (1904).
35. S. M. Sze, and K. K. Ng, *Physics of semiconductor devices* (John Wiley & Sons, 2006).
36. L. Huldt, "Band-to-band auger recombination in indirect gap semiconductors," Phys. Status Solidi A **8**, 1 (1971).
37. E. Yablonovitch, D. L. Allara, C. C. Chang, T. Gmitter, and T. B. Bright, "Unusually low surface-recombination velocity on silicon and germanium surfaces," Phys. Rev. Lett. **57**, 249 (1986).
38. S. A. Maier, *Plasmonics: fundamentals and applications* (Springer, 2007).

1. Introduction

Active control of heat flow has long been of interest in various fields [1–13]. The possibility to modulate radiative transfer is especially interesting due to its noncontact nature. The simplest mechanism to actively control radiative transfer by modulating the temperature of the emitter is limited to relatively low frequencies [14]. More quantitatively, consider the use of an optical beam to modulate the temperature of a radiative emitter. Assuming the light is absorbed near the sample surface, the amplitude of the temperature change of the film is given by $\Delta T = Q_0/\sqrt{\kappa C\omega}$, where Q_0 is the input power density, κ is the thermal conductivity, C is the volumetric heat capacity and ω is the external modulation angular frequency [15]. Let us take the input power density $Q_0 = 10^2$ Wcm^{-2}, $\kappa = 1$ Wm^{-1}K^{-1}, $C = 10^6$ Jm^{-3}K^{-1} and $\omega = 2\pi\times10^5$ rad/s. The amplitude of the temperature oscillation of the films is only about 1.3 K corresponding to a small heat transfer modulation of 8.0×10^{-4} Wcm^{-2} despite the large input power density. Thus simply modulating the temperature of a radiative emitter does not result in substantial radiative flux modulation as frequency increases.

Prior works aimed to overcome this limitation by, for example, altering emissivity with temperature-dependent phase-change materials [7, 8], carrier-injection-induced modification of

band structure in quantum wells [1], and electrostatic gating of graphene plasmonic resonators [9], among other schemes. However, these schemes modulated the far-field radiation which significantly limits the maximum heat flux. Further, the broadband nature of thermal radiation imposes stringent requirements on any method as a wide spectrum of electromagnetic waves must be manipulated.

On the other hand, near-field radiative transfer is capable of supporting heat fluxes that are orders of magnitude larger than that in the far-field [16–20] through a relatively narrow bandwidth [21]. These properties have been exploited in various applications, including thermophotovoltaics [22–25], solid-state cooling [4], thermal rectification [2,26], and active extraction of bound surface waves [5], among others. A method that is capable of dynamically modulating near-field radiative heat transfer would be of great interest. As doped semiconductors possess surface resonance frequencies in the infrared that vary with carrier concentration [27], actively altering carrier concentration could provide a mechanism to modulate radiative transfer. However, although optical pumping has been used for tuning the permittivity of different materials via carrier photoinjection with high speed [28–30], the effects on radiative transfer have not yet been studied.

Here, we propose a scheme for dynamically controlling near-field radiative transfer between semiconductors by external optical illumination with hundreds of kHz. A change of carrier concentration induced by the optical pumping shifts the plasma frequency of the semiconductor, altering the near-field radiative heat transfer coefficient. Our results show that heat transfer coefficient can be tuned from near zero to 600 $\mathrm{Wm^{-2}K^{-1}}$ at room temperature with a bandwidth on the order of hundreds of kHz. Our work introduces a promising method to realize dynamic external control of heat flow.

2. Theory

The system we consider is shown in Fig. 1. Two parallel porous silicon films (denoted as Region 1 and 2) are put in close proximity to each other with a vacuum gap distance d (denoted as Region 3). The two films are supported by two substrates in contact with separate thermal reservoirs. We choose porous silicon rather than fully dense silicon to enable the formation of surface plasmon polaritons (SPPs) with high near-field energy density as discussed in the next section. Optical elements composed of porous silicon have been fabricated for gradient refractive index devices [31] and distributed Bragg reflectors [32] in the visible regime. These two films are optically pumped by two laser beams with wavelength 400 nm corresponding to an absorption coefficient of 1.06×10^5 $\mathrm{cm^{-1}}$. Although the absorption depth is around 100 nm, smaller than the thickness of the films (1 μm), the fast carrier diffusion process on the order of 1 ns leads to a nearly uniform free carrier concentration in the film during modulation with period over 1 μs. The background doping concentration is taken to be 10^{15} $\mathrm{cm^{-3}}$. We assume that the steady power of the lasers and the temperatures of the thermal reservoirs are chosen so that each film is at a specified temperature. For the purpose of calculating the heat transfer coefficient, the temperatures of the two films are taken to be T_1 = 300 K and T_2 = 299 K, but in an actual application the temperature difference could be much larger. Under external optical pumping, excited free carriers result in the change of its relative permittivity, leading to an increase of near-field radiative heat transfer. Moreover, when the pumping is off, carriers recombine and the radiative heat transfer decreases to near zero, providing a mechanism to rapidly modulate near-field radiative transfer.

We calculate the near-field radiative heat transfer coefficient for this scheme using the standard formalism of fluctuational electrodynamics [33]. The heat transfer coefficient (h) is given as:

$$h = \frac{1}{\pi^2}\int_0^\infty d\omega \frac{\partial\Theta(\omega,T)}{\partial T}\int_0^\infty d\beta[\Gamma_s(\omega,\beta)+\Gamma_p(\omega,\beta)]. \quad (1)$$

where $\Theta(\omega,T) = \hbar\omega/[\exp(\hbar\omega/k_BT)-1]$ is the mean energy of a harmonic oscillator, $\hbar$ is the

Optics EXPRESS

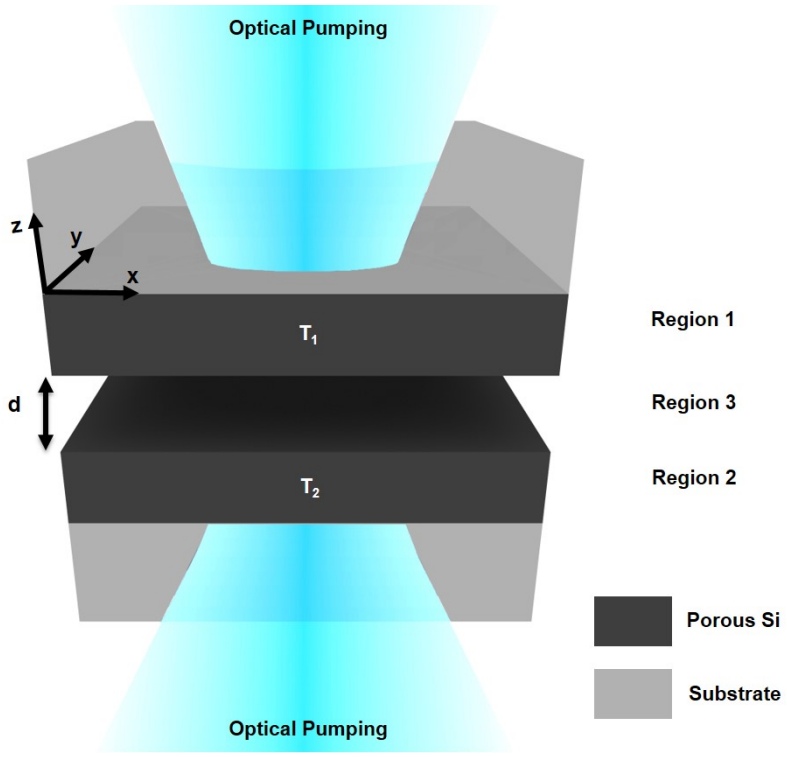

Fig. 1. Schematic of the configuration for near-field radiative transfer dynamically controlled by external optical excitation. The two porous semiconductor films of thickness t on two substrates are maintained at constant temperature of T_1 and T_2 ($T_1 > T_2$) with a vacuum gap distance of d. Free carriers are excited by the external illumination from both sides, leading to the formation of surface plasmons and resulting in a modulation of near-field radiative heat transfer.

reduced Planck constant, k_B is the Boltzmann constant, β is the wave vector in the x-y plane and T is the absolute temperature. The exchange function Γ for the s and p modes in the second integral is expressed as:

$$\Gamma_{\alpha=s,p}(\omega,\beta) = \begin{cases} \beta\dfrac{(1-|R_\alpha^1|^2)(1-|R_\alpha^2|^2)}{4|1-R_\alpha^1 R_\alpha^2 e^{i2\beta_z d}|^2}, & \text{for } \beta < \omega/\text{c}; \\ \beta\dfrac{Im[R_\alpha^1]Im[R_\alpha^2]e^{i2\beta_z d}}{|1-R_\alpha^1 R_\alpha^2 e^{i2\beta_z d}|^2}, & \text{for } \beta > \omega/\text{c}. \end{cases} \tag{2}$$

Here, R_α^i is the reflection coefficient of the multilayer system as seen from inside the vacuum gap, where i denotes the domain with i = 1, 2 and α denotes the polarization. We neglect the difference of electromagnetic properties with temperature, leading to $R_\alpha^1 = R_\alpha^2$. β_z is the wave vector along the z-direction inside vacuum. The contribution of both propagating ($\beta < \omega/c$) and evanescent waves ($\beta > \omega/c$) to the radiative transfer are included.

The effective permittivity of the porous silicon films is obtained using the Maxwell-Garnett equation [34]:

$$\epsilon_1 = \epsilon_2 = \epsilon_{eff} = \epsilon_m \frac{2f(\epsilon_i - \epsilon_m) + \epsilon_i + 2\epsilon_m}{2\epsilon_m + \epsilon_i + f(\epsilon_m - \epsilon_i)}. \tag{3}$$

where $\epsilon_m = \epsilon_\infty - \omega_p^2/(\omega^2 + i\gamma\omega)$ is the relative permittivity of the matrix medium (silicon) [27]

Optics EXPRESS

and ϵ_i is the relative permittivity of the inclusions (vacuum, $\epsilon_i = \epsilon_3 = 1$), and f is the porosity or the volume fraction of the inclusions. The plasma frequency (ω_p) is directly related to the carrier concentration which is controlled by the external illumination intensity. The effect of illumination is thus modeled simply as an altered permittivity of the porous silicon matrix.

The external optical power needed to create a steady state concentration of photoexcited carriers depends on the relevant carrier recombination mechanisms of silicon. A Shockley-Read-Hall (SRH) model is used for the trap-assisted recombination as shown in the following equation. The electron and hole lifetime parameters are assumed to be $\tau_n = \tau_p = 10$ μs with a trap density of 5×10^{13}cm^{-3} [35].

$$R_{SRH} = \frac{np - n_i^2}{\tau_p(n + n_i) + \tau_n(p + n_i)}V \tag{4}$$

with n and p being the concentrations of electrons and holes, n_i being the intrinsic carrier concentration and V being the volume of the solid portion of the porous medium. Auger recombination is also included as:

$$R_{Auger} = (C_n n + C_p p)(np - n_i^2)V \tag{5}$$

where the factor $C_n = C_p = 2\times10^{-32}$ cm^{6}s^{-1} [36].

Surface recombination is included using:

$$R_{Surface} = S(p - p_0)A_s \tag{6}$$

with S being the surface recombination velocity, p_0 being the initial concentration of holes and A_s being the surface area. The surface recombination velocity is obtained from Ref. [37]. To account for the large surface area of porous materials, we assume that the pores are spheres with radius r arranged in period of a with porosity $f = 4\pi r^3/3a^3$ which leads to a large surface to volume ratio $A_s/V = 4\pi r^2/a^3$. Although the large surface area leads to appreciable surface recombination, we note that even if the surface recombination velocity is an order of magnitude larger than the value chosen here, the required optical power to achieve a given modulation only increases by a factor of two due to the influence of Auger recombination. Therefore, our scheme is still applicable even for less ideal surfaces.

3. Results

We first examine the heat transfer coefficient versus porosity for a specific carrier concentration in Fig. 2(a). For these calculations, the carrier concentration and film thickness are chosen to be 10^{19} cm^{-3} and 1 μm, respectively. The maximum heat transfer coefficient of 640 Wm^{-2}K^{-1} is achieved at $f = 0.87$. Previously, porous silicon with porosity of 0.85 has been experimentally realized [31]. Here, we set $f = 0.80$ for future calculations. As shown in Figure 2(b), lower values of f lead to a decrease of the overall spectral heat flux value and shifts the peak of the spectral heat flux to higher frequency for which the thermal occupancy is smaller, leading to a lower heat transfer coefficient according to Equation 1. On the other hand, a higher value of f indicates less silicon and more vacuum, resulting in lower spectral heat flux, decreasing the heat transfer coefficient. We note that the optimal value of f for maximum heat transfer coefficient depends on temperature and carrier concentration.

Figure 2(c) plots the heat transfer coefficient versus thickness of the films. With a film thickness larger than 1 μm, the heat transfer coefficient remains almost constant at 600 Wm^{-2}K^{-1}. For subsequent calculations, we assume the thickness of the films to be 1 μm unless specifically specified.

External optical pumping leads to the excitation of free carriers inside the films. The curve in Fig. 2(d) depicts the carrier concentration as a result of external pumping. At low input

Optics EXPRESS

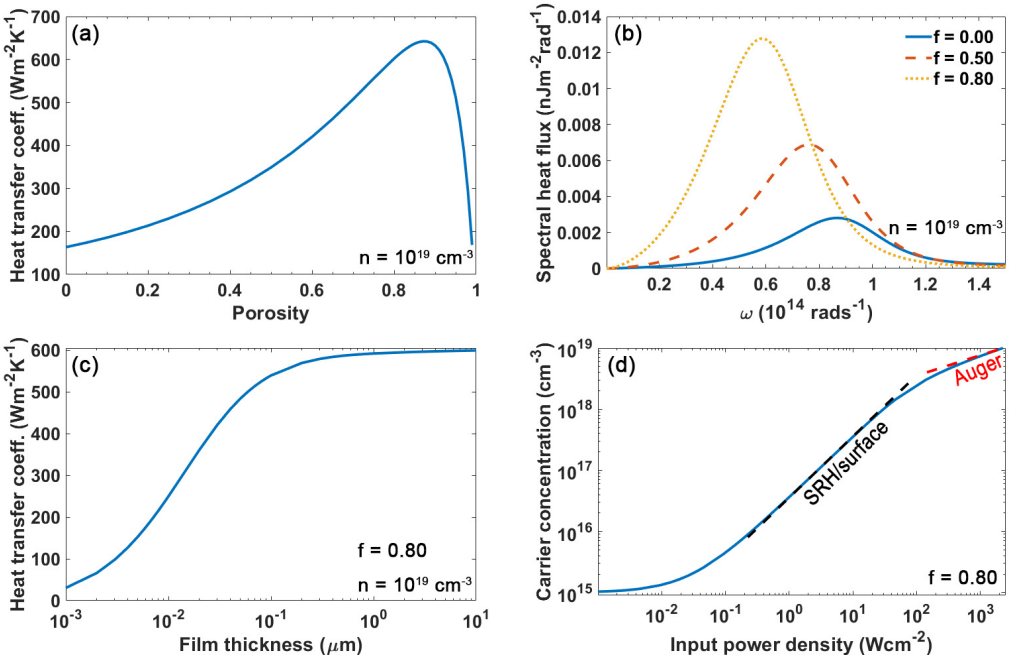

Fig. 2. (a) Heat transfer coefficient versus porosity. (b) Spectral heat flux versus frequency for different porosities. (c) Heat transfer coefficient versus film thickness at $f = 0.80$. The heat transfer coefficient remains almost constant beyond 1 μm. (d) Carrier concentration versus input power density. The black and red dashed lines are the asymptotes considering only trap-assisted/surface recombination mechanism and Auger recombination mechanisms, respectively. All the calculations in (a), (b) and (c) are performed with a carrier concentration of 10^{19} cm^{-3}

power, the carrier concentration remains at 10^{15} cm^{-3} because of background doping. An increase in the optical excitation power leads to an increase in free carrier concentration with the steady-state value determined by the recombination mechanisms. The required input power density first increases linearly with the carrier concentration in the region from 1×10^{16} to 1×10^{18} cm^{-3} where the trap-assisted recombination and surface recombination dominates at lower carrier concentrations. However, for carrier concentrations beyond 5×10^{18} cm^{-3}, a dramatic increase of input power density is needed to maintain the carrier concentration because the Auger recombination becomes the dominant recombination mechanism.

The heat transfer coefficient versus external optical power is shown in Fig. 3(a). A large variation in heat transfer coefficient is observed as the pumping power is varied. Without pumping, the heat transfer coefficient is near zero. This low heat transfer coefficient results from the absolute positive value of the silicon permittivity with negligible imaginary part for the background doping of 10^{15} cm^{-3}, resulting in little emission or absorption in the infrared wavelengths. As the carrier concentration increases due to the increased optical pumping, the real part of the silicon permittivity at low frequency becomes negative while the imaginary part increases. The material is able to support surface plasmons which contribute to the near-field radiative transfer. The maximum heat transfer coefficient is 600 Wm^{-2}K^{-1} for the considered input powers occurs at an input power density of 2.3×10^{3} Wcm^{-2}.

We now compare the modulation depth of our scheme to those in prior reports. Previously, dynamic tuning of emissivity was reported with modulation of emissivity from 0.24 to 0.74 through intersubband absorption [1] and from 0.5 to 0.95 with reconfigurable microelectromechanical

Optics EXPRESS

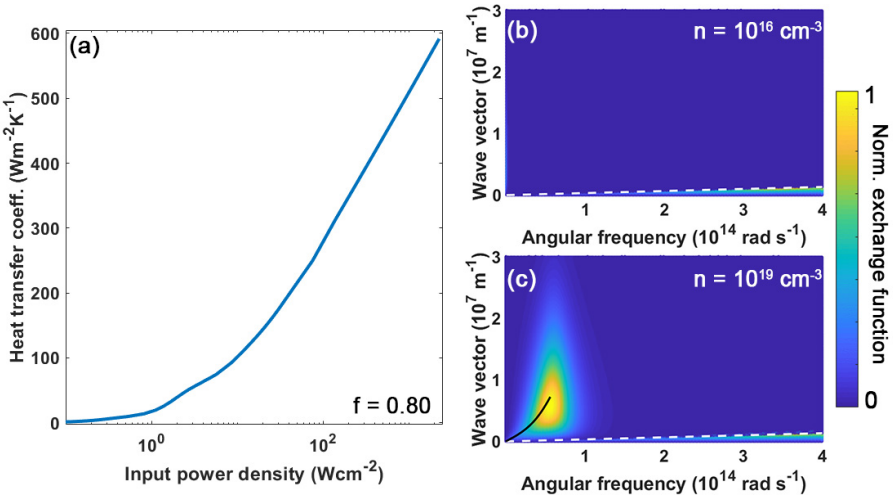

Fig. 3. (a) Heat transfer coefficient versus input power density with $f = 0.80$. The heat transfer coefficient is nearly zero at low optical pumping and increases to 600 $\mathrm{Wm^{-2}K^{-1}}$ with power density of 2.3×10^3 $\mathrm{Wcm^{-2}}$. (b) and (c) Normalized exchange function versus angular frequency and wave vector. The carrier concentration is set at (b) 10^{16} $\mathrm{cm^{-3}}$, (c) 10^{19} $\mathrm{cm^{-3}}$ with $f = 0.80$. The black solid curve in (c) denotes the dispersion relation of the SPP mode where the real part of ϵ_1 is negative. The white dashed line is the light line in vacuum. Significant enhancement of heat transfer coefficient results from the increase of exchange function in (c) compared with (b).

systems [6] in the far field, corresponding to heat transfer coefficients of 1.5 to 4.5 $\mathrm{Wm^{-2}K^{-1}}$ and 3.1 to 5.8 $\mathrm{Wm^{-2}K^{-1}}$ around room temperature. In the near field, Ref. [7] reported dynamic modulation of radiative heat transfer coefficient from 17 to 30 $\mathrm{Wm^{-2}K^{-1}}$ via phase-change material with a gap distance of 370 nm. To compare with this latter result, we recalculated the maximum variation in heat transfer coefficient for a gap distance of 370 nm. With our scheme, a modulation of heat transfer coefficient from near zero to 44 $\mathrm{Wm^{-2}K^{-1}}$ can be achieved for the same gap distance, substantially larger than that reported earlier.

We investigate the origin of the modulation by calculating the exchange function, Eq. (2), versus angular frequency and wave vector in Figs. 3(b) and 3(c). For films with carrier concentration of 10^{16} $\mathrm{cm^{-3}}$, only propagating waves under the light line contribute to radiative transfer, leading to negligible heat transfer coefficient. However, for films with carrier concentration of 10^{19} $\mathrm{cm^{-3}}$, enhanced radiative heat transfer occurs in the near field as a result of the increase in exchange function appearing above the light line, as pointed out in [27]. Thus, the heat transfer coefficient increases quickly from 5 $\mathrm{Wm^{-2}K^{-1}}$ at a carrier concentration of 10^{16} $\mathrm{cm^{-3}}$ to 600 $\mathrm{Wm^{-2}K^{-1}}$ at a carrier concentration of 10^{19} $\mathrm{cm^{-3}}$.

To further investigate the origin of the heat transfer coefficient at a carrier concentration of 10^{19} $\mathrm{cm^{-3}}$, we examine the surface mode supported by two infinitely thick porous silicon slabs. The dispersion relation of the SPPs supported in this geometry can be described by $\tanh(k_3 d/2) = -(k_3\epsilon_1)/(k_1\epsilon_3)$ and $\tanh(k_3 d/2) = -(k_1\epsilon_3)/(k_3\epsilon_1)$, where $k_j = \sqrt{k_{SPP}^2 - k_0^2\epsilon_j}$ is the wave vector in z-direction within corresponding medium with $j = 1, 3$ [38]. In the electrostatic limit ($k_{SPP} \gg \omega/c$), the dispersion relation is simplified as follows

$$k_{SPP} \approx \frac{1}{d}\ln\left(\pm\frac{\epsilon_1(\omega)-\epsilon_3}{\epsilon_1(\omega)+\epsilon_3}\right). \tag{7}$$

We superimposed the results from the dispersion relation in Fig. 3(c) as the black solid line in

Optics EXPRESS

the region where the real part of ϵ_1 is negative. It is clear that the dispersion relation matches with the peak values of the exchange function, confirming that the broadband SPP mode with high propagation constant is responsible for the enhanced heat transfer coefficient.

Next, we consider some typical values for relevant parameters for an experimental study. We take the films to have dimensions 1 cm × 1 cm, separated by a 100 nm gap. The two films are maintained at temperature of 300 and 500 K, respectively. With a tuning input power from zero to 2 W, we find that the heat transfer power can be tuned from near zero to 0.8 W. This result is significantly improved over previous results regarding the modulation depth [1, 6, 7] and exceeds the blackbody limit for radiative transfer for the same temperatures by nearly a factor of three.

Finally, we consider the maximum bandwidth of modulation of the radiative flux. Modulation by simply changing the temperature of an emitter with a modulated heat flux becomes increasingly challenging as frequency increases as discussed in the introduction. In contrast, the bandwidth of our scheme is limited only by the recombination lifetime. A tradeoff exists between bandwidth and required optical power as a shorter recombination time implies high bandwidth but requires more power to maintain a given free carrier concentration. For the parameters chosen here, at a carrier concentration of 10^{18} cm^{-3}, the lifetimes corresponding to trap-assisted, surface and Auger recombination are around 20, 1.8 and 23 μs, respectively, leading to a modulation bandwidth of around 600 kHz. Generally, the maximum modulation frequency will be on the order of hundreds of kHz for typical values of recombination lifetimes, which is faster than or comparable to previous results [1, 6, 7, 14].

4. Conclusion

In summary, we have proposed a dynamic modulation scheme for near-field radiative transfer using free carrier changes induced by external optical pumping. For the materials considered here, we show that the heat transfer coefficient can be tuned from near zero to around 600 Wm^{-2}K^{-1} with bandwidths of hundreds of kHz. Our work introduces a promising method to address the challenge of dynamic external control of heat flow.

Funding

US Department of Energy, Office of Science, Office of Basic Energy Sciences (DE-SC0001293).